

**Flow Regime Visualization and Identification of Air-Water
Two-Phase Flow in a Horizontal Helically Coiled
Rectangular Channel**

CHENG, Lixin

Available from Sheffield Hallam University Research Archive (SHURA) at:

<https://shura.shu.ac.uk/28397/>

This document is the Accepted Version [AM]

Citation:

CHENG, Lixin (2021). Flow Regime Visualization and Identification of Air-Water Two-Phase Flow in a Horizontal Helically Coiled Rectangular Channel. Heat Transfer Engineering, 43 (8-10). [Article]

Copyright and re-use policy

See <http://shura.shu.ac.uk/information.html>

Flow Regime Visualization and Identification of Air-Water Two-Phase Flow in a Horizontal Helically Coiled Rectangular Channel

Bo Cai^{a,b}, Guodong Xia^{a*}, Lixin Cheng^{a,c} and Zhipeng Wang^a

^aBeijing Key Laboratory of Heat Transfer and Energy Conversion, Beijing University of Technology,
Beijing 100124, P. R. China

^bCollege of Locomotive and Rolling Stock Engineering, Dalian Jiaotong University, Liaoning 116028, P.
R. China

^cDepartment of Engineering and Mathematics, Sheffield Hallam University, City Campus, Howard Street,
Sheffield S1 1WB, UK

Abstract

Experiments of flow regime visualization and identification of air-water two-phase flow were conducted in a horizontal helically coiled rectangular channel. The test superficial liquid and gas velocities are 0.09 - 2 m/s and 0.18 - 16 m/s, respectively. Flow regimes were observed with a high-speed video camera and the corresponding local and average void fractions were measured with an electric conductivity probe method and with a quick-close valve method, respectively. Four main flow regimes including unsteady pulsating flow, bubbly flow, intermittent flow and annular flow were observed. The bubbly flow identification criteria depend on more than 90% bubbles whose chord length smaller than the channel equivalent diameter. The annular flow identification criteria is

the local void fraction in the gas core larger than 0.97. Then the flow regimes and their transition mechanisms are analyzed. Furthermore, new transition criteria among these flow regimes have been proposed. The results show that the critical transition average void fraction from bubbly to intermittent flow is 0.23. A complete air-water flow regime map has been developed for the horizontal helically coiled rectangular channel and the map predicts the observed flow regimes well.

*Address correspondence to Prof. Guodong Xia, Beijing Key Laboratory of Heat Transfer and Energy Conversion, Beijing University of Technology, Beijing, 100124, P. R. China. E-mail: xgd@bjut.edu.cn.

Introduction

Gas-liquid two-phase flow in helically coiled channels are important in various industrial applications such as chemical process and reaction engineering, power engineering, nuclear reactors, oil-gas process system, gas-liquid mixing units, refrigeration, air conditioning and heat pump systems. However, the gas-liquid two-phase flow phenomena in helically coiled channels are very complicated due to its unique channel structure. In general, the secondary flow caused by the centrifugal acceleration has a significant impact on the momentum and mass transfer of two-phase flow in helically coiled channels, which provides an effective way to separate the phases and enhance heat transfer [1]. As the basis to understand the complicated two-phase flow phenomena in such channels, knowledge of flow regimes is important to understand the physical mechanisms of momentum and heat transfer in helically coiled channels. Although the great effort has been made to investigate the physical two-phase structure of flow regimes in straight tubes using both experimental and simulation methods over the past decades [2 - 4], less research on the gas-liquid two-phase flow in helically coiled channel has been conducted so far [5, 6]. Moreover, the investigations on two-phase flow regimes in helically coiled rectangular channels are very limited in the literature but such channels are also important in many industrial applications [7, 8].

Some researchers conducted the gas-liquid two-phase flow experiments in vertical helically coiled channels to identify the two-phase flow regimes and their transition mechanisms [9 - 12]. Various flow patterns such as stratified, slug, plug, wavy, churn and annular flow were observed in their study. Murai et al. [11, 12] observed three flow regimes including bubbly flow, slug flow and plug flow in the vertical helical coiled tubes by using the visualization method. Thandlam and Mandal

[13] conducted an experimental investigation on gas and non-Newtonian fluids in a helical tube and observed three flow regimes including plug flow, slug flow and stratified flow by using a high speed camera. They analyzed the effect of tube diameter, coiled diameter and pitch length on flow regime transitions. In recent decades the high-speed visualization method has been one of the most important ways for two-phase flow regimes identification for helically coiled channels. But more effective ways for flow regime recognition such as the electric conductivity probe method have been applied by some researchers to achieve more accurate flow regime transition boundaries. Zhu et al. [14] identified six flow regimes including bubbly, plug, slug, slug annular, wavy and annular flow in a vertical helical coiled channel with three coil diameters of 0.2, 0.4 and 0.8 m by applying the both visualization method and electric conductivity method. Furthermore, they experimental investigated the transition mechanism of the bubbly-intermittent (BI) transition [15].

Some researchers conducted the simulation studies on the two-phase flow characteristics in helical channels [7, 8, 16 - 19]. Liu et al. [16] investigated the effects of buoyancy and centrifugal force on heat transfer of supercritical CO₂ in a helically coiled tube at various inclination angles. The effects of curvature and torsion of helical tubes on the pressure distribution and liquid holdup distribution of two-phase flow were also investigated in upward and downward helical pipes by the researchers [7, 8, 17]. Moreover, the entrance effect on two-phase flow in vertical helical coils was investigated by Saffari et al. [18]. Kong et al. [19] observed the bubble traveling paths in a helically coiled tube in different injection locations. They analyzed the effects of drag force, gravitational force and centrifugal force on the bubble behaviors.

Furthermore, the flow regime transition mechanisms of two-phase flow in helically coiled tubes

have been studied by some researchers. The transition mechanisms from bubble flow to intermittent flow (BI) occurs owing to the coalescence of small bubbles or cup bubbles because the buoyancy force dominates the two-phase flow [20, 21]. It is also found that the BI transition is closely related with a critical averaged void fraction. For upward two-phase flow the critical averaged void fraction for BI transition is in the range of 0.2 - 0.52 depending on the sub-bubbly flow regimes, such as cap bubble or dispersed bubble [22 - 24]. However, the BI transition in a helical channel is largely affected by centrifugal acceleration. Li et al. [15] indicated that the BI transition in a helically coiled tube occurs at a smaller critical averaged void fraction than in the straight tube. This may be because the centrifugal force remarkably promoted the process of bubble agglomeration and coalescence. For annular flow prediction Taitel et al. [25] proposed a model to predict annular flow based on the minimum gas velocity required to impede the liquid droplets from falling. Other widely used transition mechanism for annular flow is the liquid slug or liquid bridge are destroyed by the gas core [26].

According to the afore-going literature review, limited studies of gas-liquid two-phase flow regimes in the horizontal helically coiled rectangular channel are available so far. Therefore, it is essential to conduct the experimental studies to understand the flow structures of various flow regimes together with their transition mechanisms and criteria.

The objectives of this study are to experimentally investigate the flow regimes using flow visualization method with the high-speed video camera, to simultaneously measure the local and average void fractions corresponding to the observed flow regimes to understand the flow regime transition mechanisms and to develop a complete flow pattern map in the horizontal helically coiled

rectangular channel.

Experimental system and data measurement

The two-phase flow experimental system was designed to observe two-phase flow regimes and measure the local and average void fractions simultaneously in a horizontal helically coiled rectangular channel by using the high-speed camera, the electric conductivity probe method and the quick-close valve (QCV) method. The experimental setup and test coiled rectangular channel are respectively described here.

Experimental system

The schematic diagram of the experimental setup of air-water two-phase flow for the test channel is presented in Fig. 1. It consists of the air and water supply system, a test section, a measurement system and a data acquisition system. Water is supplied by a centrifugal pump from a water tank having a volume of 1 m³. The volumetric flow rate of water is measured by an electromagnetic flow-meter with an accuracy of $\pm 0.5\%$. The water flow rate can be adjusted with an adjustable valve in the water supply line to a desired superficial liquid velocity in the experiments. Air is supplied by an air compressor and then stored in an air reservoir at a pressure of 0.8 MPa. The reservoir is used to maintain a stable gas flow rate in the experimental system. The volumetric flow rate of air is measured by three gas flow-meters with an accuracy of $\pm 1.5\%$. The three flow meters are used to achieve the wide range test range of superficial velocities from low to high values. Three valves after the gas flow meters are used to adjust the gas flow rate to a desired superficial gas

velocity in the experiments. Air and water are well mixed in a Y-connection mixer before the test section, which has a straight branch for liquid flow and air injected in the side-way. The pipe between the Y-mixer and the test section is long enough to ensure that the gas-liquid two-phase flow is stable in the experiments. Then, the air-water two-phase mixtures flow into the test section which is the horizontal helically coiled rectangular channel, where the local void fractions were measured with the electric conductivity probe method and the corresponding flow regimes were simultaneously observed with the high-speed video camera. The average void fractions were also measured for the flow regimes with the QVC method. The measured data were taken by a data acquisition system and a computer. Finally, the two-phase fluids flow back to the water tank which is open to the atmosphere. The water returns to the water tank and the air vents into the atmosphere.

The test section is a transparent helically coiled rectangular channel which is made of plexiglass. Figure 2 shows the schematic diagram of the helically coiled rectangular channel with its main geometry dimensions. Table 1 lists the geometry dimensions of the test section corresponding to Fig. 2. The coil diameter D of the helically coiled channel is 141 mm and its pitch P is 140 mm. The helix angle of the test section is 0.306 rad. The dimensions of the rectangular cross-section of channel is: $w \times h = 25$ mm (width) \times 34 mm (height). The two-phase flow structures are obtained by the high-speed video camera at four axial positions ($\theta = 360^\circ, 450^\circ, 540^\circ$ and 630°) along the second turn of channel. The visualization photos with 512×512 pixels are acquired at a frequency of 250 - 2500 Hz and the acquiring time is 4.1 - 33.2 s.

The measurement uncertainties were analyzed with the methods proposed by Taylor [27] in this study. Table 2 shows the summary of the uncertainties of measurement parameters. The processing

precisions of the width and height of rectangular cross-section of channel are less than 0.5 mm. the area uncertainty of rectangular cross-section of channel is estimated to be about 1.18%. The uncertainty of superficial liquid velocity is $\pm 3.22\%$. The uncertainty of superficial gas velocity is $\pm 5.99\%$.

Measurement, data reduction method and uncertainties

Measurements of the local void fractions and observing the corresponding flow regimes with the high-speed video camera were simultaneously taken in the experiments. The visualization method has been an important way to identify two-phase flow regimes, but this method has subjectivity. The electric conductivity probe method is a more accurate flow pattern recognition way by using the quantitatively criteria such as the bubble length and local void fraction.

Figure 3 (a) shows the schematic diagram of the electric conductivity probe used in the measurement of the local void fraction in the test section and Figure 3(b) illustrate the measurement positions in the rectangular channel. The electric conductivity probe can discriminate the gas and liquid phases by measuring the conductivity of the two-phases when the probe tip is submerged in the phases. A total of 13 local void fractions can be measured at the same time as shown in Fig. 3(b). The in-house electric conductivity probe was manufactured by positioning a stainless steel needle (O.D. 0.25 mm) into a supporting tube (O.D. 1.2 mm) as illustrated in Fig. 3(a). The needle surface except the tip was electrically insulated by an overlay of capillary insulation. The probe is an L shape with the tip facing the two-phase flow direction. A circuit of the probe supplies a DC voltage between the needles and the supporting tube. The phase discriminate passage shifted from output signals of

the circuit was sampled by an A/D converter at a sampling frequency of 1 kHz. The acquiring period of the measurement is 150 s for detecting sufficient data for further analysis. The measurement of the time-averaged local void fraction was conducted at the thirteen radial positions at $\theta = 540^\circ$ (indicated in Fig. 1) by translating the probe along the y-direction as illustrated in Fig. 3(b).

The raw output voltage signals $V(t)$ from the probe is represented as a dashed line in Fig. 3 (c) under intermittent flow condition. When the probe tip is merged into the gas phase the low voltage signals are outputted because the resistance of air is extremely high. When the probe tip is merged into the liquid phase the high voltage signals are outputted owing to the strong conductivity of water. The single-threshold technique (Tyagi and Buwa [28], Zhai et al. [29]) were used to convert the raw output signal into the square wave signal. Base on the visualization method the threshold for bubbly and intermittent flow was calibrated and the threshold value TV is set as $0.75 \cdot \text{MAX} [V(t)]$. The phase discriminate function of square wave signal can be expressed as follows:

$$P(t) = \begin{cases} 0 & \text{for } V(t) \leq TV & \langle \text{is the gas phase} \rangle \\ 1 & \text{for } V(t) > TV & \langle \text{is the liquid phase} \rangle \end{cases} \quad (1)$$

Research on bubble length distribution becomes an effective way to build the transition boundary from bubbly to intermittent flow [14]. The length of bubbles can be obtained from the velocity of bubbles and their resident time. The resident time Δt_i of the i th bubbles passing through the needle tip can be calculated from the phase discriminate function $P(t)$. The size of i th bubble can be acquired by the velocity of bubbles acquired by visualization method and the resident time. The

correlation for calculating the i th bubble chord length is as follows:

$$l_{B,i} = \Delta t_i v \quad (2)$$

where, v is average velocity of bubbles, which is acquired by visualization method, Δt_i is the resident time of i th bubble. The time-averaged local void fraction in the gas core is an important parameter to identify the annular flow. The time-averaged local void fraction at a given position in the sampling time T is calculated by

$$\alpha(y) = \frac{1}{T} \sum_{i=1}^n \Delta t_i \quad (3)$$

where $\alpha(y)$ is the local void fraction at a given axial and radial location, n is the sampling size of bubbles. The average void fractions corresponding to the respective flow regimes were measured with the QCV method and the details of the methods and results can be referred to the work of Xia et al. [30].

The local void fractions were measured corresponding to various flow regimes which were simultaneously observed by the high-speed camera. Experiments of air-water two-phase flow were conducted at a temperature of 20°C. Table 3 lists the experimental conditions covering a wide range of superficial liquid and gas velocities. The superficial liquid velocity varies from 0.11 to 2 m/s and the superficial gas velocity varies from 0.18 to 16 m/s.

Results and mechanisms of flow regime visualization and identification

The two-phase flow structures and the evolution of different flow regimes are analyzed through the experimental observations of flow regimes together with the corresponding local void fractions. Visualization analysis is one of the most widely used approach to identify the flow regimes but its disadvantage is subjective. Therefore, the electric conductivity probe technique was used to distinguish the flow regimes and understand the physical mechanisms of flow regime evolution. The measurements using the electric conductivity probe for each flow regime were made at axial position of 540° . The identification criteria of the flow regimes and their physical mechanisms are analyzed here. Furthermore, a complete flow regime map has been proposed for the helically coiled rectangular channel.

Unsteady pulsating flow regime

The unsteady pulsating flow regime is a special flow regime only found in the horizontal helically coiled channel. Figure 4 shows the observed flow regimes and the probe signals of the unsteady pulsating flow acquired at $\theta = 540^\circ$ in the coiled channel at the indicated conditions. This flow regime often happens at low superficial liquid and gas velocities. Under this flow regime the gas phase occupies the upper part of the channel for a while, and the rest lower part is occupied by the liquid phase. After a moment the liquid phase from the inlet increases gradually and eventually flows through the whole channel. The definition of this flow regime is derived from the flow features that the mixture passing through the channel every few seconds has analog to pulsating flow. The

evolution and main features of this flow regime are described as: At the beginning of 3.4 s, the liquid phase is followed by the gas phase flow through the channel as shown in Fig. 4a (i) at the superficial gas velocity of 0.85 m/s and the superficial liquid velocity of 0.245 m/s; At 3.725 s, the field of view is full of the gas phase as shown in Fig. 4a (ii); At 4.05 s, the liquid phase appears close to the inner wall as shown in Fig. 4a (iii); Finally until 4.375 s the accumulated liquid phase under the action of pressure rapidly passes through the channel as shown in Fig. 4a and then one period pulsating flow is completed.

The probe output signals for unsteady pulsating flow regime are achieved simultaneously for different superficial liquid velocities of 0.098 m/s and 0.245 m/s shown in Figs. 4(b) and (c), respectively. It is shown that the gas and liquid phases alternate flow through the probe with an unsteady pulsating period. The air flows through the channel as a pure gas phase rather than the gas slugs or the gas core. And the liquid phase with a bubble entrainment is also detected by the probe. Due to the effect of the gravity force, the probe detected more liquid phase near the inner wall ($y = 2$ mm) than that in the outer wall region ($y = 32$ mm). With increasing the superficial liquid velocity, the pulsating frequency increases and the gas occupying field reduces, which eventually leads to the transition from unsteady pulsating flow to intermittent flow.

Bubbly flow regime

The bubbly flow happens at low gas flow rate and high liquid flow rate. Discrepancy of various forces, such as gravity, buoyancy, inertia and other forces, exerting on the mixture results in various flow behavior of bubbles in different positions of the channel. The bubble behavior at the second turn

of the helical channel (from $\theta = 360^\circ$ to 630°) at different gas and superficial liquid velocities are illustrated in Fig. 5 (a) ($U_{SG} = 0.1$ m/s and $U_{SL} = 0.605$ m/s) and Fig. 5 (b) ($U_{SG} = 0.163$ m/s and $U_{SL} = 1.176$ m/s). The evolution and main features are described as: (i) At the axial position of 360° , the bubbles are squashed in flat shape and the bubbles flow close to the inner wall region due to the gravity and centrifugal effects; (ii) At $\theta = 450^\circ$, the bubbles grow bigger and the gap between the bubbles is observed due to the liquid inverse flow; (iii) At $\theta = 540^\circ$, the bubbles grow further, the bubbles flow near the outer wall of the channel, which indicates the centrifugal force controls the flow; (iv) At $\theta = 630^\circ$, the big bubbles flow slowly and bubble coalescence phenomenon probably happens.

The output signals of the probe for bubbly flow regime are achieved for different superficial liquid velocities shown in Fig. 5 (c) ($U_{SG} = 0.327$ m/s, $U_{SL} = 1.01$ m/s) and Fig. 5 (d) ($U_{SG} = 0.327$ m/s, $U_{SL} = 1.07$ m/s), respectively. It can be seen that a large number of small bubbles are detected by the probe tip for a very short resident time. The gas bubble chord lengths are smaller than channel height. With increasing the superficial liquid velocity, the discrete bubbles are scattered into uniformly dispersed bubbles by the liquid turbulence shown in Fig. 5(b). Moreover, the enhanced centrifugal effect induces more liquid phase to flow near the outer wall of the channel and the bubbles are pushed to the inner wall. At a higher superficial liquid velocity, more small bubbles are closer to the inner wall shown in Fig. 5 (d) ($U_{SG} = 0.327$ m/s and $U_{SL} = 1.07$ m/s) compared to that in Fig. 5 (c) ($U_{SG} = 0.327$ m/s and $U_{SL} = 1.01$ m/s). This indicates the two-phase bubble flow in helical channel is dominated by centrifugal effect in high liquid flow rate, but at low liquid flow rate the bubble flow is also affected by the gravity effect.

The bubbly flow region in flow regime map is determined by Zhu et al. [14] depending on more than ninety percent of bubbles whose chord length smaller than the tube diameter. In this study the channel equivalent diameter d_E is used to divide the small and elongated bubbles. The criterion of the bubbly flow identification is as follows:

$$P(l_B) = \frac{n_{l_B \leq d_E}}{n} \geq 0.9 \quad (4)$$

where $n_{l_B \leq d_E}$ is the number of bubbles whose chord length smaller than the channel equivalent diameter, n is the number of total bubbles at a sampling time. The distributions of bubble chord length which obtained at measuring position of $y = 7$ mm are presented in Fig. 5 (e) ($U_{SG} = 0.163$ m/s and $U_{SL} = 0.588$ m/s) and Fig. 5 (f) ($U_{SG} = 0.163$ m/s and $U_{SL} = 1.176$ m/s). It can be found that the chord length of the most bubbles are smaller than the channel equivalent diameter.

Intermittent flow regime

Figures 6 (a) - (b) shows the intermittent flow evolution along the second turn of the channel at different superficial liquid velocities. According to the observed results in Fig. 6 (a) ($U_{SG} = 1.307$ m/s and $U_{SL} = 0.441$ m/s), the evolution and flow characteristics of intermittent flow are described as: (i) At axial position of 450° , slender Taylor bubbles flow close to inner wall are formed; (ii) At $\theta = 540^\circ$, the Taylor bubbles became bigger because some centrifugal force is cancelled out by gravity force; (iii) At $\theta = 630^\circ$, due to the effect of the buoyant force, the velocity of Taylor bubbles decreases

and the width of Taylor bubbles increases. The Taylor bubble coalescence occurs; (iv) At $\theta = 360^\circ$, more small bubbles appear in the gas-liquid two-phase interface due to the strong secondary flow generated in the coiled channel.

The output signals of the probe for intermittent flow regime are achieved for different superficial liquid velocities shown in Fig. 6 (c) ($U_{SG} = 1.209$ m/s, $U_{SL} = 1.01$ m/s) and Fig. 6 (d) ($U_{SG} = 1.209$ m/s, $U_{SL} = 0.605$ m/s), respectively. The gas slugs and the liquid slugs with a bubble entrainment are alternate flow through the probe. Almost all the gas slugs are longer than the channel height. As shown in Fig. 6(b) ($U_{SG} = 1.307$ m/s and $U_{SL} = 0.827$ m/s), at a higher superficial liquid velocity, the strong secondary flow induces more liquid phase to shift to the outer wall region, which pushes the Taylor bubbles to the inner wall region. The processed probe signals under different flow rates for intermittent flow are shown in Fig. 6 (c) ($U_{SG} = 1.209$ m/s and $U_{SL} = 0.605$ m/s) and Fig. 6 (d) ($U_{SG} = 0.654$ m/s and $U_{SL} = 0.83$ m/s). With increasing the superficial liquid flow velocity from 0.65 to 0.83 m/s, less gas component is captured by the electric conductivity probe, and the resident time of Taylor bubbles decreases. Fig. 6 (e) ($U_{SG} = 1.209$ m/s and $U_{SL} = 0.523$ m/s) and Fig. 6 (f) ($U_{SG} = 0.654$ m/s and $U_{SL} = 0.817$ m/s) present the Taylor bubbles length distributions at the port of $y = 17$ mm for different liquid flow velocities. With increasing the superficial liquid velocity, the Taylor bubble length distribution becomes more peak and the peak Taylor bubble length decreases.

Annular flow regime

Figures 7(a) and (b) present the annular flow regime evolution along the flow direction against different superficial liquid velocities. The evolution and flow characteristics of the annular flow are

described as (i) At a low superficial liquid velocity, the liquid film becomes thin and its thickness is varied along the axial direction shown in Fig. 7(a) ($U_{SG} = 9.482$ m/s and $U_{SL} = 0.196$ m/s); (ii) At a high superficial liquid velocity, the liquid film thickness on the outer wall is always larger than that on the inner wall in Fig. 7(b) ($U_{SG} = 11.441$ m/s and $U_{SL} = 0.686$ m/s). The gas-liquid two-phase interface becomes more waviness resulting from the strong secondary flow generated in the coiled channel; (iii) At $\theta = 450^\circ$, the liquid film on the outer wall is the thickest due to the gravity effect.

The output probe signals of annular flow at $\theta = 540^\circ$ of the channel are shown in Fig. 7(c) ($U_{SG} = 11.11$ m/s and $U_{SL} = 0.163$ m/s) and 7(d) ($U_{SG} = 9.15$ m/s and $U_{SL} = 0.67$ m/s). At the superficial liquid velocity of 0.6 m/s, no gas component at the port of $y = 32$ mm is captured by the electric conductivity probe, hence the thickness of the liquid film on the outer wall is larger than 2 mm. The liquid entrainment in the gas core is also detected by the probe. At a higher liquid flow rate, the liquid entrainment at ports of $y = 7$ mm and 17 mm increases.

The transition from annular flow to intermittent flow is due to the formation of liquid bridges or liquid slugs in the continuous gas core. The maximum time-averaged void fraction in the gas core for upward two-phase flow is in the range of 0.993 - 0.998 according to Vieira et al. [31]. Hence the annular flow in the present study can be identified by using the time-averaged local void fraction in the gas core larger than 0.97. The criteria of recognition of annular flow can be expressed as follows:

$$\alpha(y) \geq 0.97 \quad (5)$$

Development of flow regime map and their transition criteria

About 200 air-water flow regime observations in the horizontal helically coiled rectangular channel have been obtained under a wide range of superficial liquid and gas velocities. The observed flow regimes of unsteady pulsating flow, bubbly flow, slug flow and annular flow in the horizontal helically coiled channel are plotted in the flow map in Fig. 8. Unsteady pulsating flow is a peculiar flow regime occurring at the low liquid and gas flow rate, and it occupies the lower left-corner of the flow regime map. The transition from unsteady pulsating to intermittent flow is the boundary line of liquid phase continuous flow and discontinuous flow. The bubbly flow happens in the condition of high liquid flow depending on strong liquid turbulence. Hence bubble flow distributes in the top left corner of the flow regime map. The appearance of annular flow is in the case of the gas phase destroying the liquid bridge in formation of the continuous gas core in the center of the channel. The annular flow distributes in the right side of the map when the superficial gas velocity is almost larger than 7 m/s.

Comparisons of experimental flow regime data to the existing transition criteria

The experimental BI boundary for helically coiled channel is compared with the existing BI transitions proposed by Mandhane et al. [32], Zhu et al. [14] and Murai et al. [11] shown in Fig. 9(a). It is can be seen that the gradient of experimental BI boundary is much smaller than that of other BI boundaries, and it occurs at a lower liquid flow rate than other transitions. This is because the strong secondary flow generated in test channel is conducive to the formation of bubble flow so that BI transition happens at a lower liquid flow rate.

A comparison of the present flow transition from annular to intermittent flow (AI) boundary to

various existing AI transitions is presented in Fig. 9(b). The AI transition lines selected for the comparison are those proposed by Taitel and Bornea et al. [25], Mandhane et al. [32], Julia and Hibiki [33] and Zhu et al. [14]. It is found that the transition boundary in the helically coiled tube occurs earlier than that in straight tubes. The reason is that the centrifugal force promotes the separation of the gas-liquid two-phases. On the other hand, the annular flow regime in the horizontal helically coiled channel occurs at a higher superficial gas velocity than that in a vertical helically coiled tube. This is due to the liquid film affected by the strong secondary flow may destroy the continuous gas core and generate the liquid bridge in the test channel.

The flow regime transition criteria have been extensively studied in various tubes with different geometry structures by many researchers over the past decades. Flow regime transition criteria are strongly affected by the flow regime transition mechanisms for different flow regimes in various channels with different structures and different arrangements. In this study, new criteria to demarcating the observed flow regimes have been proposed base on the relationship between the averaged void fraction and flow regimes. The average void fraction acquired by the QCV method corresponding to the flow regimes is shown in Fig. 10.

Development of transition criteria of flow regimes

The transition mechanism from bubbly to intermittent flow regime was studied for upward two-phase flow by many researchers such as Das et al. [34] and Lucas and Kreper et al [33] etc., just to name two examples here. When the buoyancy force dominates the flow, the bubble agglomeration and coalescence is the main cause of the BI transition [36]. Base on the visualization analysis in the

present study, the mechanism of BI transition in horizontally helical two-phase flow may be interpreted as the bubble coalescence. According to the existing research, the BI transition is closely related to a critical averaged void fraction, which is independent of the gas and superficial liquid velocities. In this case, the critical average void fraction may be used to identify the flow regime changes. Thus, the critical averaged void fraction α_c for the BI transition may be expressed as follows:

$$\alpha_c = \text{constant} \quad (6)$$

Figure 10 shows the relationship between the averaged void fraction and flow regimes in the horizontal helically coiled channel. It can be found that the critical average void fraction of BI transition is around 0.23 which may be used to identify the bubbly and intermittent flow regimes. Therefore, Eq. (6) can be rewritten as following:

$$\alpha_c = 0.23 \quad (7)$$

For the horizontal helically coiled channel, the correlation for the average void fraction α has been developed by Xia et al. [30] as

$$\alpha = 0.302 \left[\left(\frac{U_{SG}}{U_{SL}} \right) \left(\frac{1}{Fr} \right) \right]^{0.2} \quad (8)$$

$$Fr = \frac{U_{SL}}{\sqrt{gd_E}} \quad (9)$$

where g is acceleration of gravity, d_E is the equivalent diameter of test channel.

Substitute Eq. (7) into (8) to obtain a correlation which may be used for calculating the BI transition boundary when the critical averaged void fraction α_c is equal to 0.23. Thus, the correlation used for predicting the BI transition for the helically coiled rectangular channel on case of $U_{SG} > 0.34$ may be expressed as follows:

$$U_{SG} = 0.256FrU_{SL} \quad (10)$$

It is worth noting that the critical averaged void fraction α_c of 0.23 in the horizontally helically coiled rectangular channel is higher than the critical average 0.065 in the vertical helically coiled tubes [14]. This indicates that the secondary flow effect is stronger for helically coiled channel in horizontally arrangement than that in vertical arrangement. This strong secondary flow may destroy the bubble coalescence and result in the BI transition occurring at a higher gas phase flow rate in horizontal helically coiled rectangular channel. The BI transition line is plotted in the average void fraction corresponding to the flow regime as shown in Fig. 10. It captures the experimental data reasonably well.

The transition mechanism from the unsteady pulsating flow to the intermittent flow regime can be explained as the inertia force of mixture overcoming the gravity force to generate the continuous two-phase flow. Therefore, the transition correlation is strongly related to the Froude number Fr

defined in Eq. (9) which represents the ratio of inertia force to the gravity force. As shown in Fig. 10, it is impossible to separate the unsteady pulsating flow and the intermittent flow by a constant value of the average void fraction. It is clear that the transition boundary is a function of superficial gas velocity. The critical average void fraction may be correlated as follows:

$$\alpha_c = 0.17U_{SG} + 0.2 \quad (11)$$

The correlation that calculates the transition boundary from unsteady pulsating flow to intermittent flow (UI) in case of $U_{SG} \geq 0.4$ m/s has been proposed as

$$U_{SG} = 1.77 \left[\left(\frac{U_{SG}}{U_{SL}} \right) \left(\frac{1}{Fr} \right) \right]^{0.2} - 1.176 \quad (12)$$

According to the relationship between the average void fractions and the corresponding flow regimes in Fig.10, the AI flow transition is independent of the average void fraction. Therefore, the AI transition criterion among the flow regimes is only dependent on the superficial gas velocity and can be expressed as follows:

$$U_{SG} = \text{constant} \quad (13)$$

According to the experimental data, the intermittent and annular boundary is around the

superficial gas velocity of 7 m/s. Therefore, the criterion for predicting the boundary from the intermittent flow to annular flow is expressed as

$$U_{SG} = 7 \text{ m/s} \quad (14)$$

The experimental data for all the four flow regimes are compared to the new proposed flow regime transition criteria as shown in Fig. 11. It can be concluded that new transition correlations have a good predictive capability to capture the measured flow regime data. The new proposed flow map is applicable for a wide range of conditions: U_{SL} and U_{SG} are in the range of 0.09 - 2 m/s and 0.18 - 16 m/s, respectively.

Conclusions

Experimental study of flow regimes of air-water two-phase flow in the horizontal helically coiled rectangular channel with flow visualization together with the simultaneous measurements of the local and average void fractions corresponding to the flow regimes. The mechanisms of flow regime transitions have been understood according to the experimental data and flow visualization analysis. Furthermore, a new flow regime map and correlations of flow regime transitions have been proposed. The following conclusions have been reached:

(1) Four main flow regimes, i.e. unsteady pulsating flow, bubbly flow, intermittent flow and annular flow are classified as the main flow regimes in the horizontal helically coiled rectangular channel. The unsteady pulsating flow regime is typical and peculiar to be defined in the helically

coiled channel with the horizontal orientation.

(2) For the helically coiled rectangular channel, it is observed that at a higher superficial liquid velocity, more liquid phase shifts to the outer side of the channel due to the centrifugal effect, which leads to the increase of liquid film thickness on the outer wall. This is used to explain the flow regime transition mechanisms in the study.

(3) The complex geometry in the horizontal helically coiled rectangular channel may result in the strong secondary flow which induces the generation of dispersed small bubbles. Thus, the bubble flow region increases in flow regime map compared with inclined tubes and vertical helically coiled tubes observed in the literature.

(4) Due to the effect of the centrifugal force generated in the coiled channel, separation the two-phases and the annular-to-intermittent flow transition occurs earlier than in those in straight tubes.

(5) According to the relations between the average void fractions and flow regimes, the transition criteria and correlations between the flow regime transitions have been proposed to distinguish the flow regime. The results show that the critical average void fraction from bubbly to intermittent flow is 0.23 and their transition boundary is $U_{SL} = 0.256FrU_{SL}$. The intermittent and annular boundary is around the superficial gas velocity of 7 m/s. The predicted flow regime transitions by these criteria and correlations have a good agreement with the experimental data.

(6) A new flow regime map has been proposed by incorporating the new flow regime transition correlations. Compared to the entire experimental flow regime data observed in this study, the flow map captures the experimental flow regimes reasonably well. The flow map is applicable to a wide range of conditions.

Nomenclature

- A Area of rectangular cross-section, m^2
- AI flow regime transition from annular to intermittent flow
- BI flow regime transition from bubbly to intermittent flow
- D coil diameter, m
- d_E equivalent diameter of test channel with rectangular cross-section, m
- Fr Froude number defined in Eq. (9)
- g gravity acceleration, m/s^2
- h height of rectangular cross-section of channel, m
- l_B bubble length, m
- n number of bubbles in sampling time
- $O.D.$ outer diameter of the channel, m
- P pitch, m
- $P(t)$ phase discriminate function
- QCV quick close valve
- Δt_i resident time of i th bubble, s
- T sampling time, s
- TV threshold value
- U_{SG} superficial gas velocity, m/s
- U_{SL} superficial liquid velocity, m/s

UI unsteady pulsating to intermittent flow

v average velocity of bubbles, m/s

$V(t)$ output voltage signal of the probe, V

w width of rectangular cross-section of channel, m

x x-coordinate defined in Fig. 2

y y-coordinate defined in Fig. 2

Greek symbols

α average void fraction of channel

α_c critical averaged void fraction

$\alpha(y)$ local void fraction at a given axial and radial location

θ axial location along the channel, $^\circ$

φ helix angle, rad

Acknowledgements

This research is funded by the National Natural Science Foundation of China (No. 51976002).

References

- [1] D. K. Nguyen, and J. Y. San, "Heat Transfer and Exergy Analysis of a Spiral Heat Exchanger," *Heat Transfer Eng.*, vol. 37, no. 12, pp. 1013-1026, 2016. DOI: 10.1080/01457632.2015.1104159.

- [2] L. Cheng, G. Ribatski, and J. R. Thome, “Two-phase flow patterns and flow-pattern maps: fundamentals and applications,” *Appl. Mech. Rev.*, vol. 61, no. 5, 50802, 28 pages, 2008. DOI: 10.1115/1.2955990.
- [3] L. Cheng, G. Ribatski, J. Moreno Quibén, and J. R. Thome, “New prediction methods for CO₂ evaporation inside tubes: Part I - A two-phase flow pattern map and a flow pattern based phenomenological model for two-phase flow frictional pressure drops,” *Int. J. Heat Mass Transfer*, vol. 51, no. 1-2, pp. 111-124, 2008. DOI: 10.1016/j.ijheatmasstransfer.2012.05.044.
- [4] L. Cheng, G. Ribatski, and J. R. Thome, “New prediction methods for CO₂ evaporation inside tubes: Part II - An updated general flow boiling heat transfer model based on flow patterns,” *Int. J. Heat Mass Transfer*, vol. 51, no. 1-2, pp. 125 - 135, 2008. DOI: 10.1016/j.ijheatmasstransfer.2007.04.001.
- [5] M. Ghobadi, and Y. S. Muzychka, “A review of heat transfer and pressure drop correlations for laminar flow in curved circular ducts,” *Heat Transfer Eng.*, vol. 37, no. 10, pp. 815-839, 2016. DOI: 10.1080/01457632.2015.1089735.
- [6] A. J. Ghajar, “Heat transfer and pressure drop in the transition region of smooth horizontal circular tubes with different inlet configurations,” *Adv. Heat Transfer*, vol. 51, pp. 1-53, May 2019. DOI: 10.1016/bs.aiht.2019.05.001.
- [7] X. F. Liu, G. D. Xia, and G. Yang, “Experimental study on the characteristics of air–water two-phase flow in vertical helical rectangular channel,” *Int. J. Multiphase Flow*, vol. 73, pp. 227-237, Mar. 2015. DOI: 10.1016/j.ijmultiphaseflow.2015.03.012.
- [8] G. D. Xia, and X. F. Liu, “An investigation of two-phase flow pressure drop in helical channel,”

- Int. Comm. Heat Mass Transfer*, vol. 54, pp. 33–41, May 2014. DOI: 10.1016/j.icheatmasstransfer.2014.03.009.
- [9] B. Gao, and Q. C. Bi, “Experimental performance comparison of shell-side heat transfer for shell-and-tube heat exchangers with different helical baffles,” *Heat Transfer Eng.*, vol. 37, no. 18, pp. 1566-1578, 2016. DOI: 10.1080/01457632.2016.1151300.
- [10] A. J. Ghajar, and L. M. Tam, “Heat transfer measurements and correlations in the transition region for a circular tube with three different inlet configurations,” *Exp. Therm. Fluid Sci.*, vol. 8, no. 1, pp. 79-90, 1994. DOI: 10.1016/0894-1777(94)90075-2.
- [11] Y. Murai, S. Yoshikawa, S. I. Toda, M. A. Ishikawa, and F. Yamamoto, “Structure of air–water two-phase flow in helically coiled tubes,” *Nucl. Eng. Des.*, vol. 236, no. 1, pp. 94-106, 2006. DOI: 10.1016/j.nucengdes.2005.04.011.
- [12] Y. Murai, K. Inaba, Y. Takeda, and F. Yamamoto, “Backlight imaging tomography for slug flows in straight and helical tubes,” *Flow Meas. Instrum.*, vol. 18, no. 5-6, pp. 223-229, 2007. DOI: 10.1016/j.flowmeasinst.2007.07.001.
- [13] A. K. Thandlam, and T. K. Mandal, “Flow pattern transition, frictional pressure drop, and holdup of gas non-Newtonian fluid flow in helical tube,” *Asia-Pac. J. Chem. Eng.*, vol. 10, no. 3, pp. 422-437, 2015. DOI: 10.1002/apj.1886.
- [14] H. Zhu, Z. Li, X. Yang, G. Zhu, J. Tu, and S. Jiang, “Flow regime identification for upward two-phase flow in helically coiled tubes,” *Chem. Eng. J.*, vol. 308, no. 15, pp. 606-618, 2017. DOI: 10.1016/j.cej.2016.09.100.
- [15] Z. X. Li, S. Y. Jiang, X. T. Yang, Y. C. Huang, and H. Y. Zhu, “Bubbly-intermittent flow transition

- in helically coiled tubes,” *Chem. Eng. J.*, vol. 323, no. 1, pp. 96-104, 2017. DOI: 10.1016/j.cej.2017.04.029.
- [16] X. Liu, X. Xu, C. Liu, J. Ye, and H. Li, “Numerical study of the effect of buoyancy force and centrifugal force on heat transfer characteristics of supercritical CO₂ in helically coiled tube at various inclination angles,” *Appl. Therm. Eng.*, vol. 116, pp. 500-515, Jan. 2017. DOI: 10.1016/j.applthermaleng.2017.01.103.
- [17] X. F. Liu, D. H. Zhao, and Y. F. Liu, “Numerical analysis of the two-phase flow characteristics in vertical downward helical pipe,” *Int. J. Heat Mass Transfer*, vol. 108, Part B, pp. 1947–1959, Jan. 2017. DOI: 10.1016/j.ijheatmasstransfer.2017.01.056.
- [18] H. Saffari, R. Moosavi, N. M. Nouri, and C. X. Lin, “Prediction of hydrodynamic entrance length for single and two-phase flow in helical coils,” *Chem. Eng. Proc.: Proc. Intensif.*, vol. 86, pp. 9-21, Nov. 2014. DOI: 10.1016/j.cep.2014.10.005.
- [19] L. J. Kong, X. Gao, R. Li, and J. Han, “Bubbles in curved tube flows-An experimental study,” *Int. J. Heat Mass Transfer*, vol. 105, pp. 180-188, Sept. 2017. DOI: 10.1016/j.ijheatmasstransfer.2016.09.064.
- [20] D. Barnea, “A unified model for predicting flow-pattern transitions for the whole range of pipe inclinations,” *Int. J. Multiphase Flow*, vol. 13, no. 1, pp. 1–12, 1987. DOI: 10.1016/0301-9322(87)90002-4.
- [21] K. Mishima, and T. Hibiki. “Some characteristics of air–water two-phase flow in small diameter vertical tubes,” *Int. J. Multiphase Flow*, vol. 22, no. 4, pp. 703–712, 1996. DOI: 10.1016/0301-9322(96)00010-9.

- [22] L. W. Ralph, and C. Kilyoan. “Two-Phase Flow Distribution to Tubes of Parallel Flow Air-Cooled Heat Exchangers,” *Heat Transfer Eng.*, vol. 26, no. 4, pp. 003-018, 2005. DOI: 10.1080/01457630590916239.
- [23] J. E. Julia, B. Ozar, J. J. Jeong, T. Hibiki, and M. Ishii, “Flow regime development analysis in adiabatic upward two-phase flow in a vertical annulus,” *Int. J. Heat Fluid Flow*, vol. 32, no. 1, pp. 164–175, 2011. DOI: 10.1016/j.ijheatfluidflow.2010.09.003.
- [24] S. S. Chougule, V. V. Nirgude, and Sahu S. K., “Experimental Study on Laminar Forced Convection of Al₂O₃/Water and Multiwall Carbon Nanotubes/Water Nanofluid of Varied Particle Concentration with Helical Twisted Tape Inserts in Pipe Flow,” *Heat Transfer Eng.*, vol. 39, no. 9, pp. 806–816, 2018. DOI: 10.1080/01457632.2017.1341235.
- [25] Y. Taitel, D. Bornea, and A. E. Dukler, “Modelling flow pattern transitions for steady upward gas-liquid flow in vertical tubes,” *AIChE J.*, vol. 26, no. 3, pp. 345–354, 1980. DOI: 10.1002/aic.690260304.
- [26] K. Mishima, and M. Ishii, “Flow regime transition criteria for upward two-phase flow in vertical tubes,” *Int. J. Heat Mass Transfer*, vol. 27, no. 5, pp. 723–737, 1984. DOI: 10.1016/0017-9310(84)90142-x.
- [27] J. R. Taylor, *An Introduction to Error Analysis*. Sausalito, CA, USA: University Science Books, 1997.
- [28] P. Tyagi, and V. V. Buwa, “Experimental characterization of dense gas–liquid flow in a bubble column using voidage probes,” *Chem. Eng. J.*, vol. 308, pp. 912–928, Sept. 2017. DOI: 10.1016/j.cej.2016.09.026.

- [29] L. S. Zhai, P. Bian, Z. K. Gao, and N. D. Jin, "The measurement of local flow parameters for gas-liquid two-phase bubbly flows using a dual-sensor probe array," *Chem. Eng. Sci.*, vol. 144, no. 22, pp. 346-363, 2016. DOI: 10.1016/j.ces.2016.01.058.
- [30] G. Xia, B. Cai, L. Cheng, and Z. Wang, "Experimental studies and modelling of average void fraction of air-liquid two-phase flow in a helically coiled rectangular channel," *Exp. Therm. Fluid Sci.*, vol. 94, pp. 9-22, Jan. 2018. DOI: 10.1016/j.expthermflusci.2018.01.027.
- [31] R. E. Vieira, M. Parsi, B. S. McLaury, and S. A. Shirazi, "Experimental characterization of vertical downward two-phase annular flows using Wire-Mesh Sensor," *Chem. Eng. Sci.*, vol. 134, no. 29, pp. 324-339, 2015. DOI: 10.1016/j.ces.2015.05.013.
- [32] J. M. Mandhane, G. A. Gregory, and K. Aziz, "A flow pattern map for gas-liquid flow in horizontal pipes," *Int. J. Multiphase Flow*, vol. 7, no. 4, pp. 537-553, 1974. DOI: 10.1016/0301-9322(74)90006-8.
- [33] J. E. Julia, and T. Hibiki, "Flow regime transition criteria for two-phase flow in a vertical annulus," *Int. J. Heat Fluid Flow*, vol. 32, no. 5, pp. 993-1004, 2011. DOI: 10.1016/j.ijheatfluidflow.2011.06.001.
- [34] G. Das, P. K. Das, N. K. Purohit, and A. K. Mitra, "Flow pattern transition during gas liquid upflow through vertical concentric annuli. I. Experimental investigations," *J. Fluids Eng. – Trans. ASME*. vol. 121, no. 4, pp. 895-901, 1999. DOI: 10.1115/1.2823553.
- [35] D. Lucas, E. Krepper, and H. M. Prasser, "Development of co-current air-water flow in a vertical pipe," *Int. J. Multiphase Flow*, vol. 31, no. 12, pp. 1304-1328, 2005. DOI: 10.1016/j.ijmultiphaseflow.2005.07.004.

[36] A. K. Das, and P. K. Das, “Modelling bubbly flow and its transitions in vertical annuli using population balance technique,” *Int. J. Heat Fluid Flow*, vol. 31, no. 1, pp. 101-114, 2010. DOI: 10.1016/j.ijheatfluidflow.2009.11.006.

Table 1. Geometry parameters of the helical coiled channel.

Parameters	Value
Channel height, h (m)	0.034
Channel width, w (m)	0.025
Pitch, P (m)	0.140
Coil diameter, D (m)	0.141
Helix angle, φ (rad)	0.306

Table 2. Uncertainties of the measured parameters.

Measurement parameters	Unit	Uncertainty
Area of rectangular cross-section A	m^2	1.18%
Superficial liquid velocity U_{SL}	m/s	3.22%
Superficial gas velocity U_{SG}	m/s	5.99%

Table 3. Experimental conditions.

Fluids	Superficial velocity (m/s)
Water	0.09 - 2.00
Air	0.18 - 16.00

List of figure captions

Figure 1. Air-water two-phase flow experimental system.

Figure 2. Schematic diagram of horizontal helically coiled channel with its main geometry dimensions.

Figure 3 The measurement method of electric conductivity probe: (a) Structure of probe, (b) Probe measurement ports and (c) Output signal of probe.

Figure 4 Visualization of unsteady pulsating flow and its flow characteristics (a) visualization images of flow regime evolution; (b) and (c) the probe output signals.

Figure 5. Visualization of bubbly flow and its flow characteristics: (a) and (b) visualization of bubbly flow evolution; (c) and (d) the probe output signals; (e) and (f) bubble chord length distribution.

Figure 6. Visualization of intermittent flow and its flow characteristics: (a) and (b) visualization of bubbly flow evolution; (c) and (d) the probe output signals; (e) and (f) bubble chord length distribution.

Figure 7. Visualization of annular flow and its flow characteristics: (a) and (b)

visualization of bubbly flow evolution; (c) and (d) the probe output signals.

Figure 8. Flow regime map of air-water flow in helically coiled channel.

Figure 9. Comparison of flow regime transition with previous works: (a) transition from bubbly to intermittent flow; (b) transition from intermittent to annular flow.

Figure 10. Correlations of flow regime transition criteria base on the relationship between average void fraction and flow regimes.

Figure 11. Comparison of proposed flow regimes transition boundaries with experimental data.

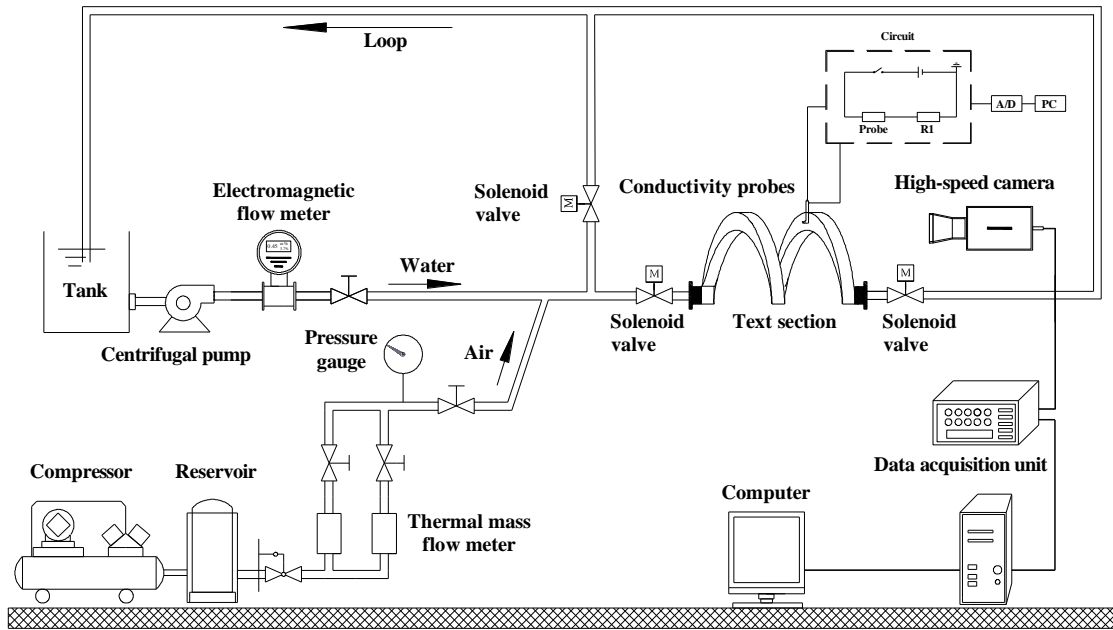


Figure 1. Air-water two-phase flow experimental system.

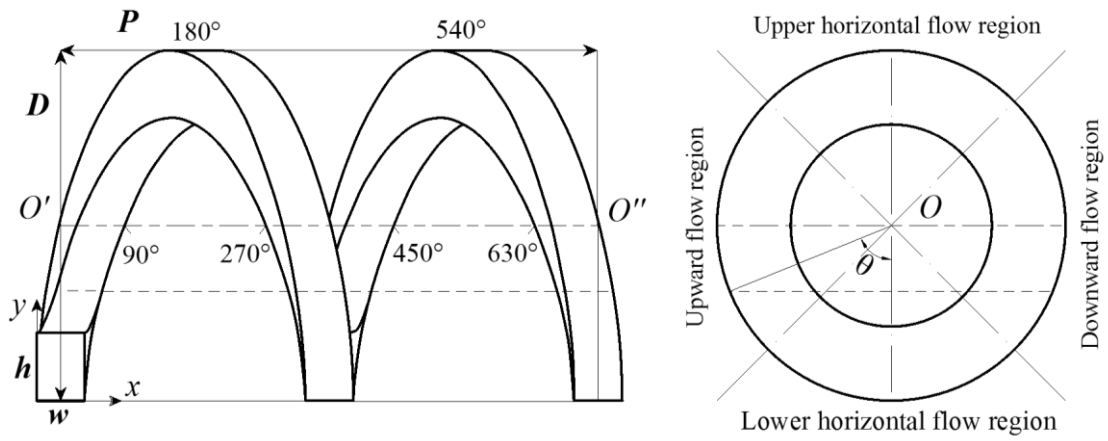


Figure 2. Schematic diagram of horizontal helically coiled channel with its main geometry dimensions.

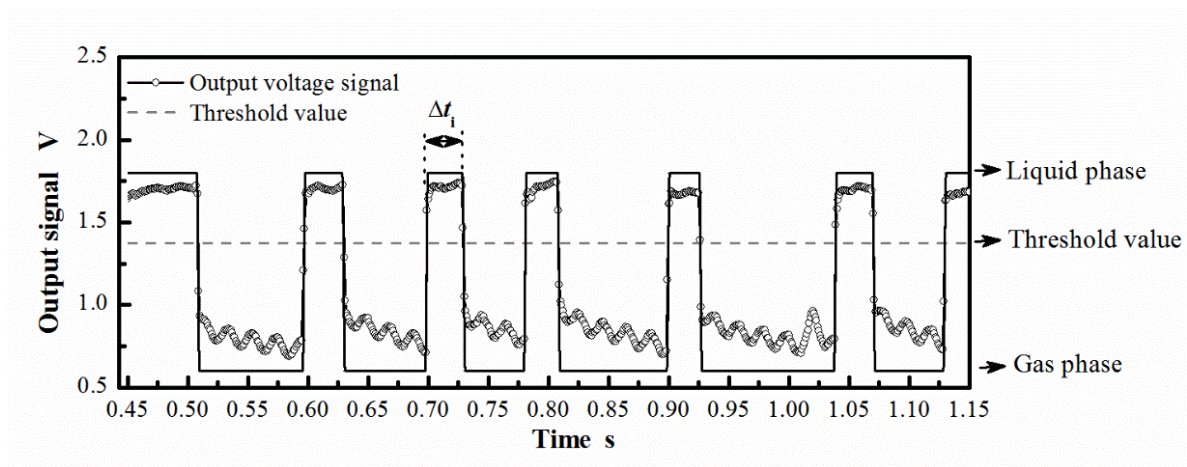
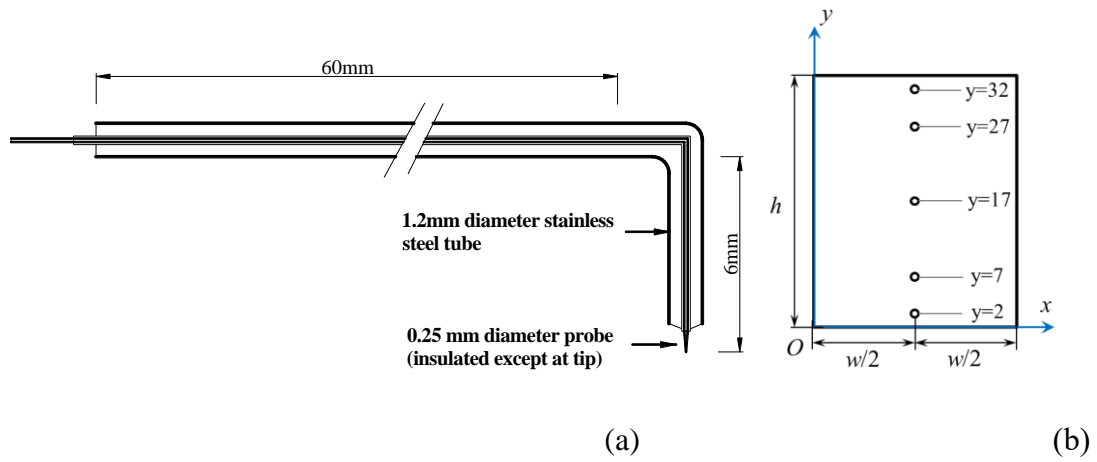
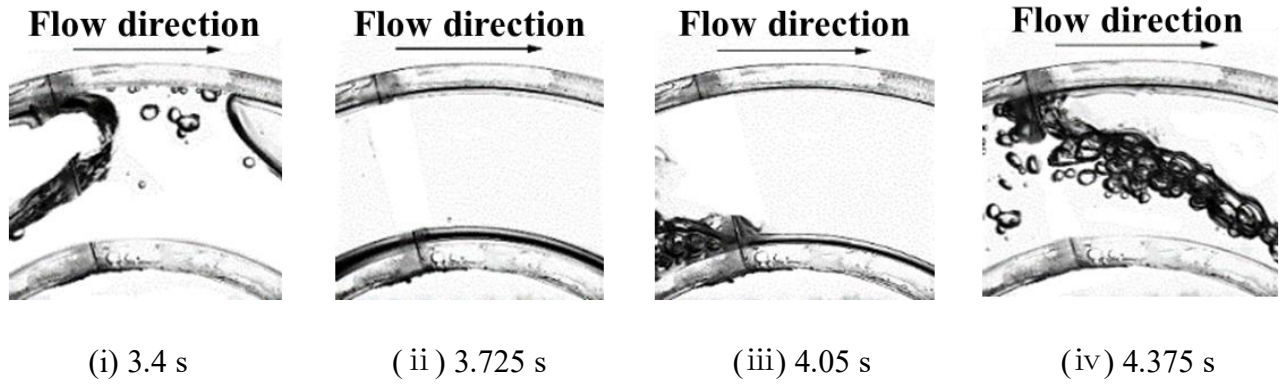
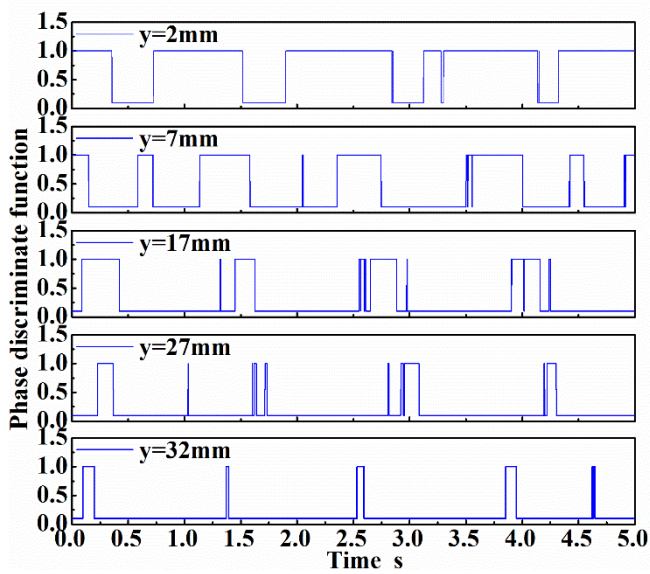


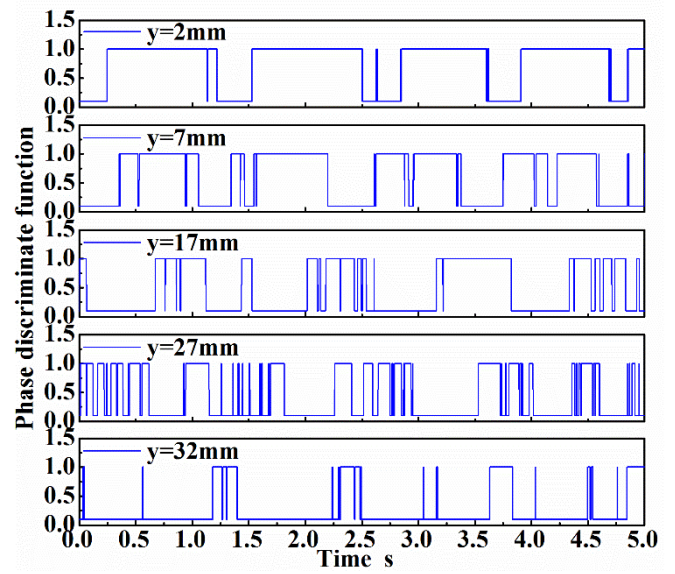
Figure 3. The measurement method of electric conductivity probe: (a) Structure of probe, (b) Probe measurement ports and (c) Output signal of probe.



(a) $U_{SG} = 0.85$ m/s, $U_{SL} = 0.245$ m/s

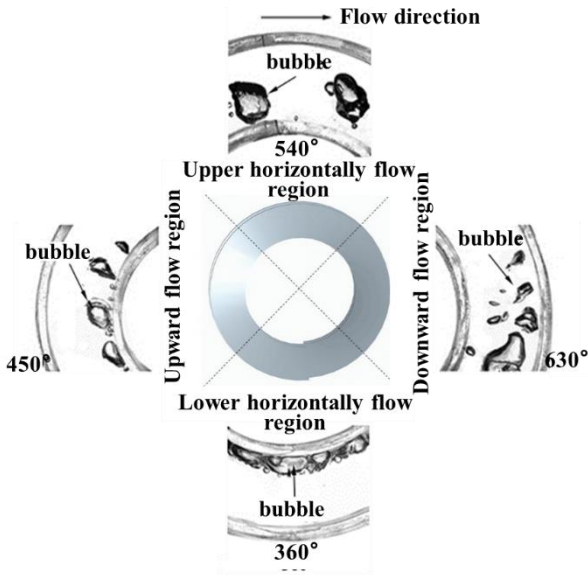


(b) $U_{SG} = 0.85$ m/s, $U_{SL} = 0.098$ m/s

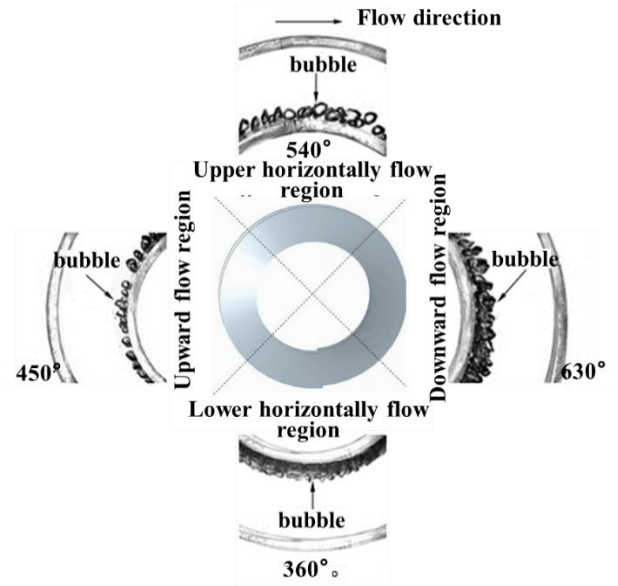


(c) $U_{SG} = 0.85$ m/s, $U_{SL} = 0.245$ m/s

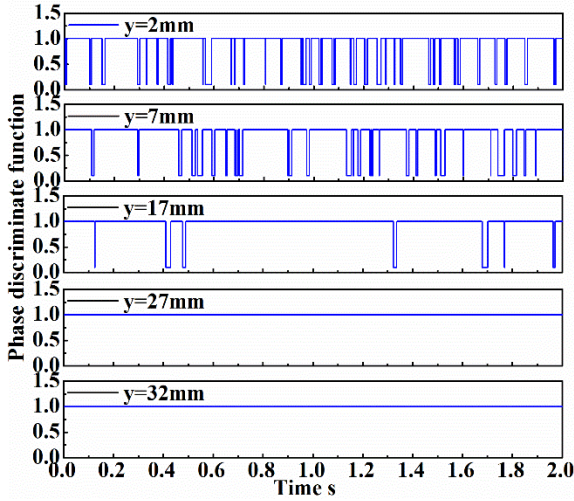
Figure 4. Visualization of unsteady pulsating flow and its flow characteristics: (a) visualization images of flow regime evolution; (b) and (c) the probe output signals.



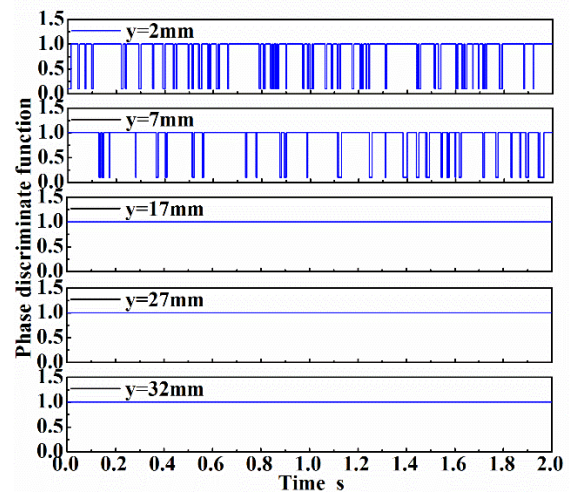
(a) $U_{SG} = 0.10$ m/s, $U_{SL} = 0.605$ m/s



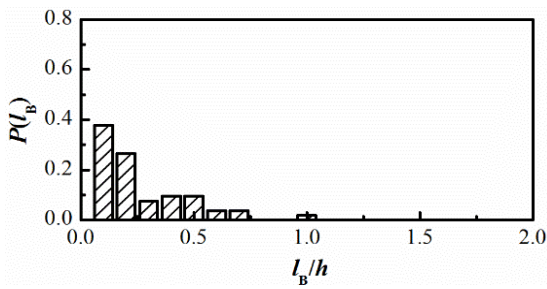
(b) $U_{SG} = 0.163$ m/s, $U_{SL} = 1.176$ m/s



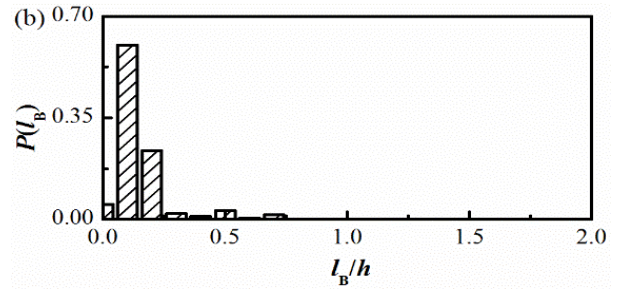
(c) $U_{SG} = 0.327$ m/s, $U_{SL} = 1.01$ m/s



(d) $U_{SG} = 0.327$ m/s, $U_{SL} = 1.07$ m/s

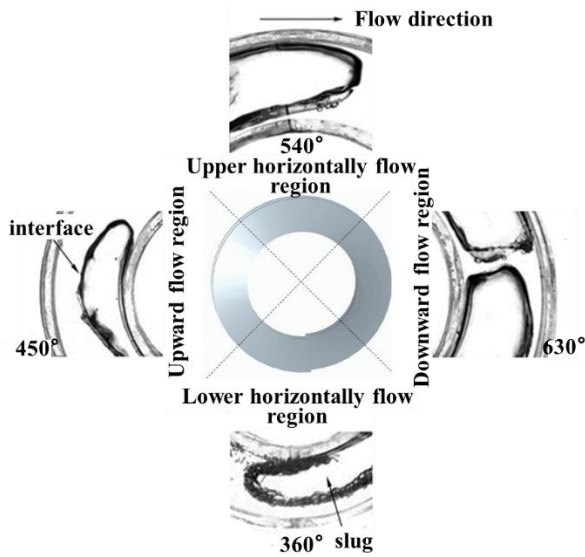


(e) $U_{SG} = 0.163$ m/s, $U_{SL} = 0.588$ m/s

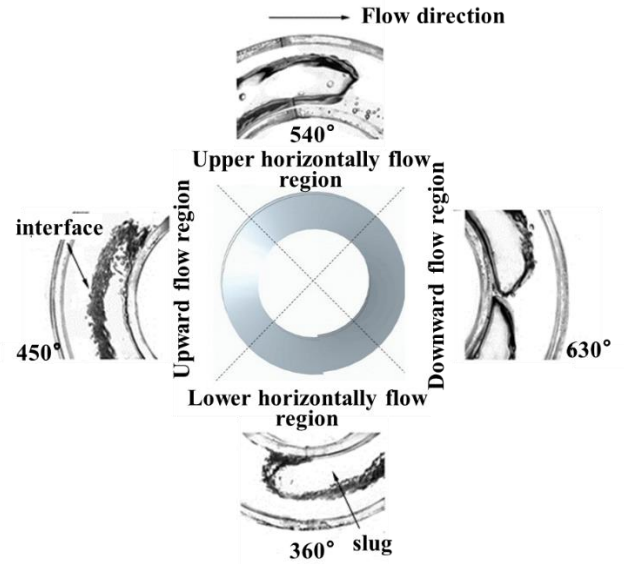


(f) $U_{SG} = 0.163$ m/s, $U_{SL} = 1.176$ m/s

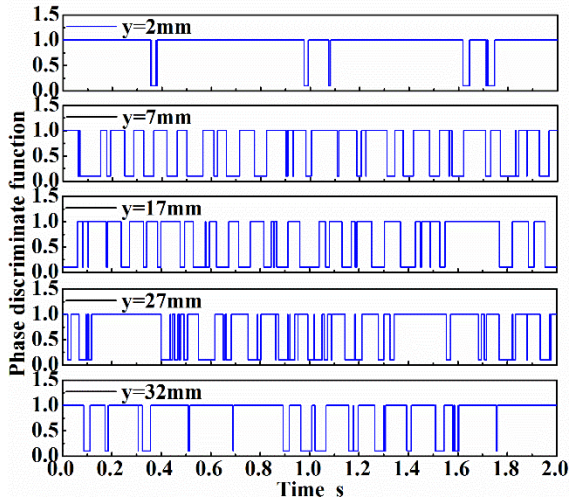
Fig. 5. Visualization of bubbly flow and its flow characteristics: (a) and (b) visualization of bubbly flow evolution; (c) and (d) the probe output signals; (e) and (f) bubble chord length distribution.



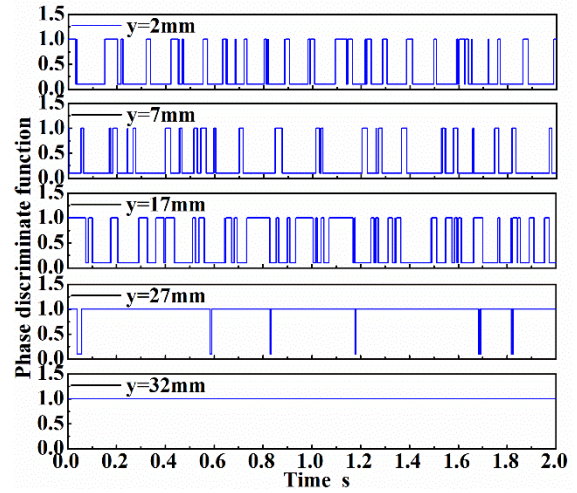
(a) $U_{SG} = 1.307$ m/s, $U_{SL} = 0.441$ m/s



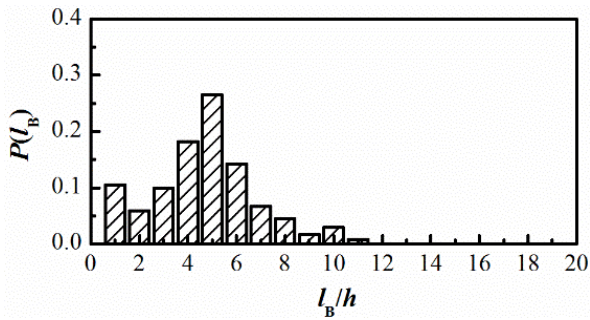
(b) $U_{SG} = 1.307$ m/s, $U_{SL} = 0.827$ m/s



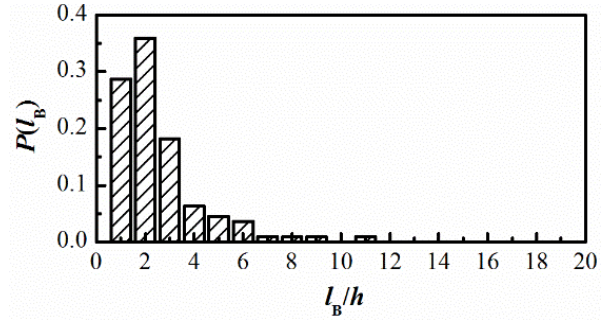
(c) $U_{SG} = 1.209$ m/s, $U_{SL} = 1.01$ m/s



(d) $U_{SG} = 0.129$ m/s, $U_{SL} = 0.605$ m/s

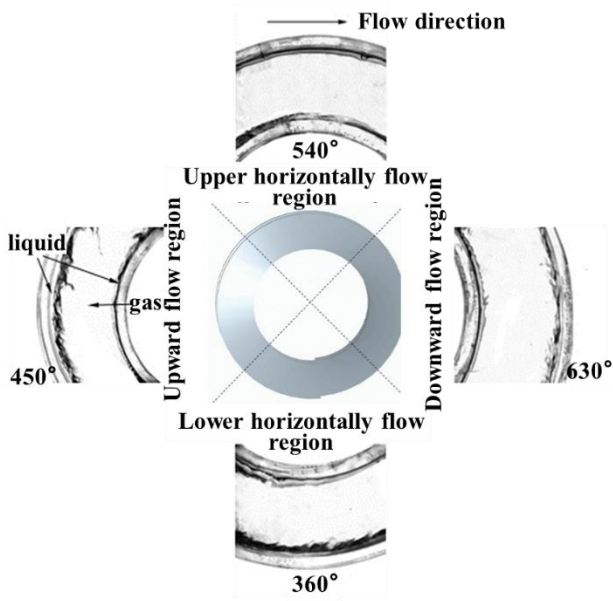


(e) $U_{SG} = 1.209$ m/s, $U_{SL} = 0.523$ m/s

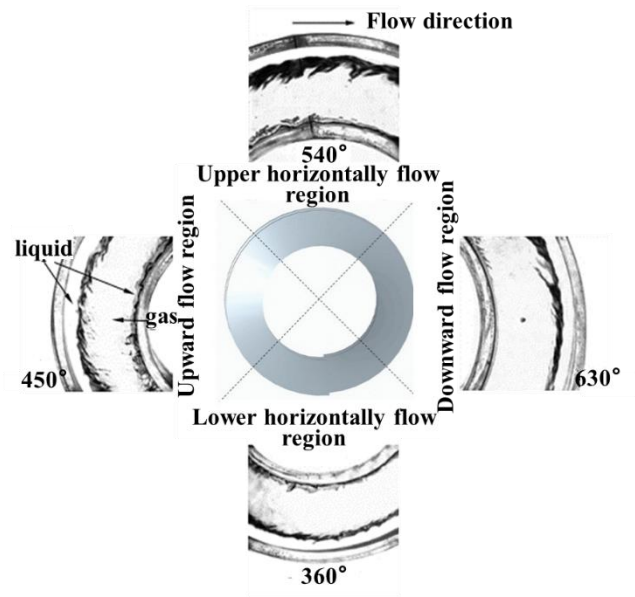


(f) $U_{SG} = 1.209$ m/s, $U_{SL} = 0.817$ m/s

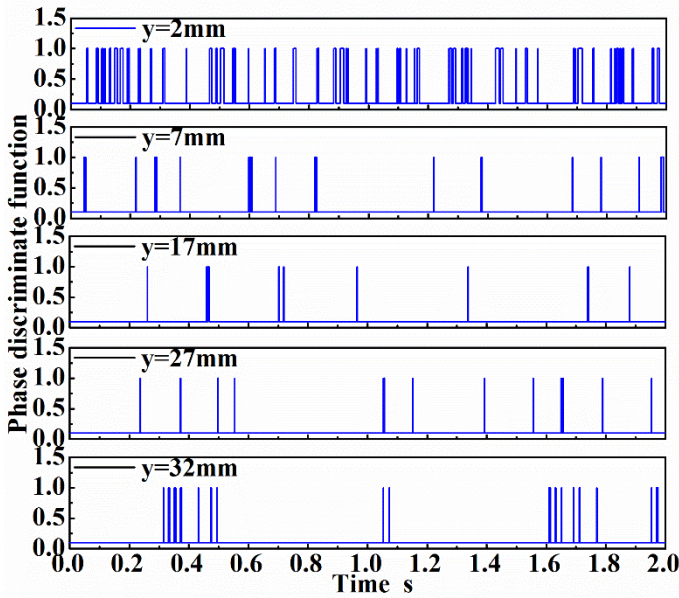
Fig. 6. Visualization of intermittent flow and its flow characteristics: (a) and (b) visualization of bubbly flow evolution; (c) and (d) the probe output signals; (e) and (f) bubble chord length distribution.



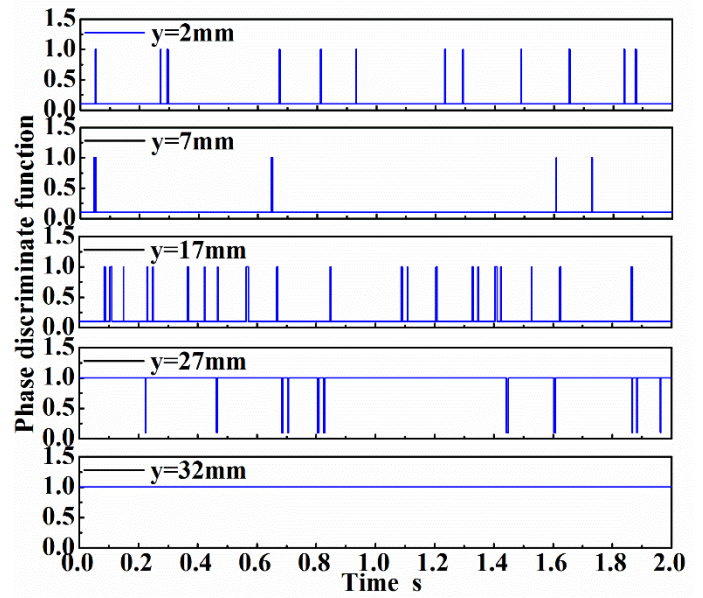
(a) $U_{SG} = 9.482 \text{ m/s}$, $U_{SL} = 0.196 \text{ m/s}$



(b) $U_{SG} = 11.441 \text{ m/s}$, $U_{SL} = 0.686 \text{ m/s}$



(c) $U_{SG} = 11.11 \text{ m/s}$, $U_{SL} = 0.163 \text{ m/s}$



(d) $U_{SG} = 9.150 \text{ m/s}$, $U_{SL} = 0.670 \text{ m/s}$

Fig. 7. Visualization of annular flow and its flow characteristics: (a) and (b) visualization of bubbly flow evolution; (c) and (d) the probe output signals.

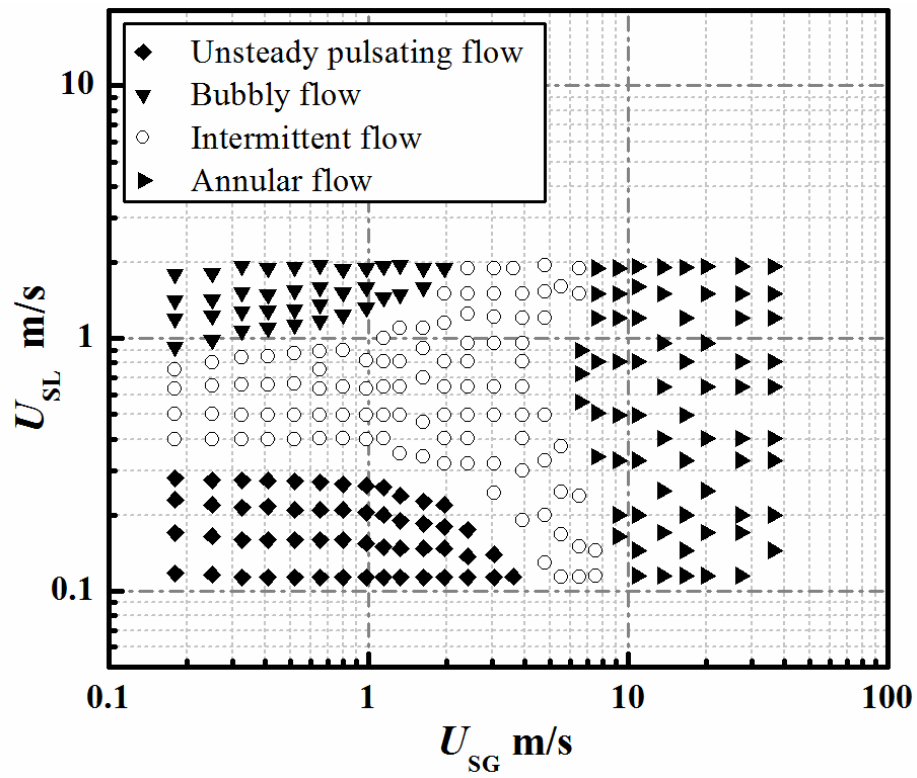
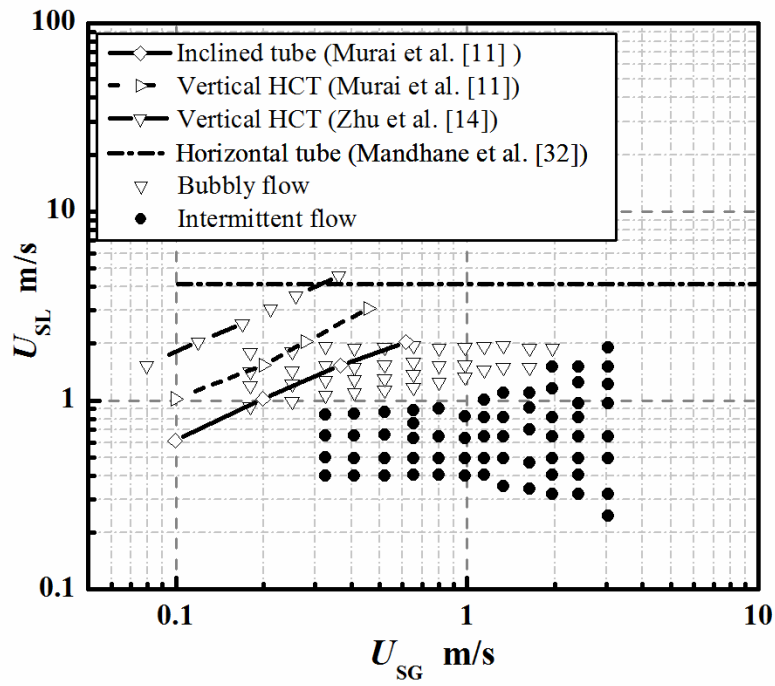
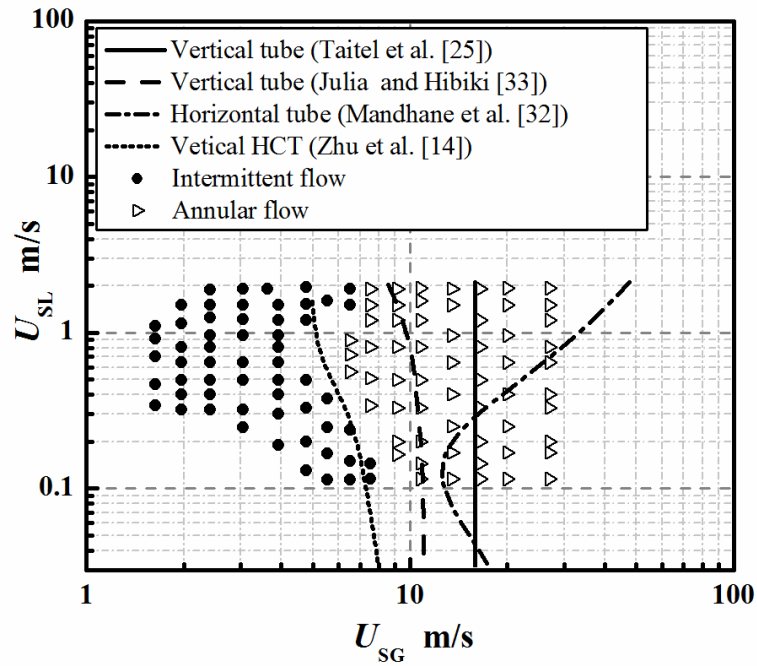


Figure 8. Flow regime map of air-water flow in helically coiled channel.



(a)



(b)

Figure 9. Comparison of flow regime transition with previous works: (a) transition from bubbly to intermittent flow; (b) transition from intermittent to annular flow.

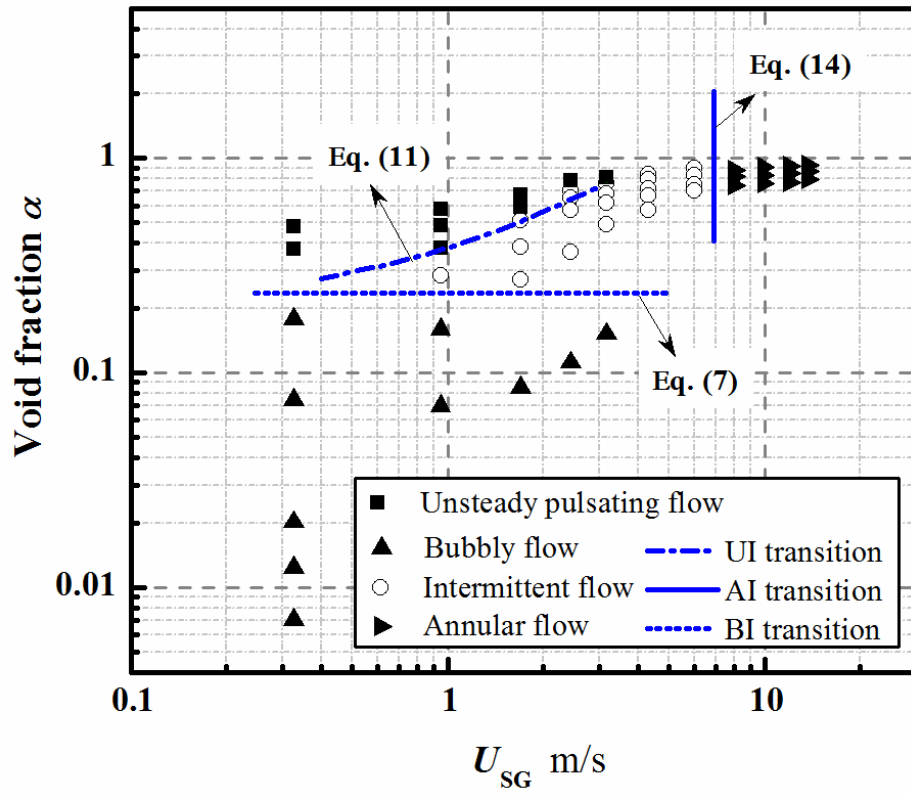


Figure 10. Correlations of flow regime transition criteria base on the relationship between average void fraction and flow regimes.

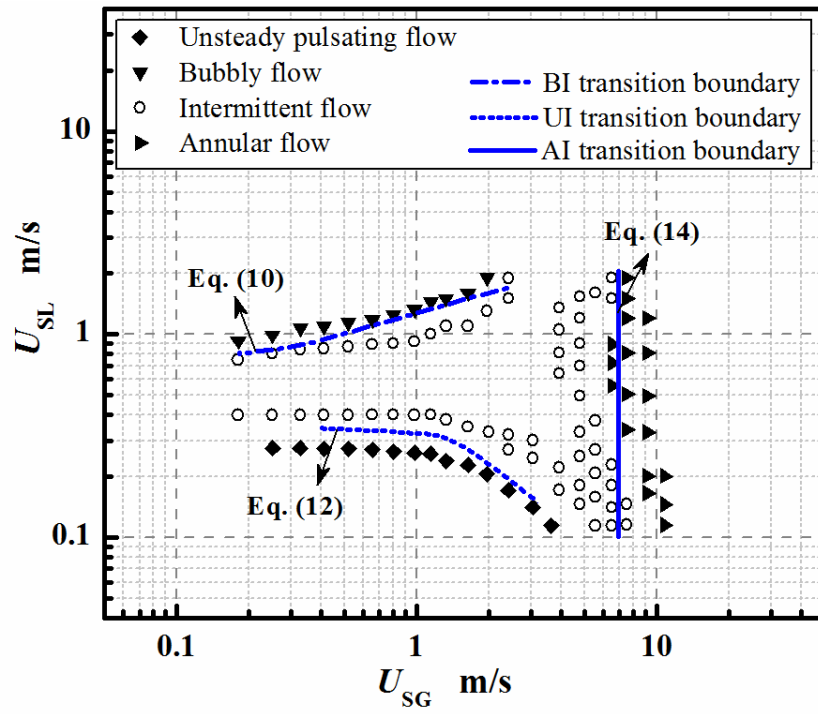


Figure 11. Comparison of proposed flow regimes transition boundaries with experimental data.

Notes on contributors



Bo Cai is a senior lecturer in the College of Locomotive and Rolling Stock Engineering at Dalian JiaoTong University. After receiving her Ph.D. in Beijing University of Technology of China, she worked as a lecturer in Dalian JiaoTong University and post-doctor in Matsushita refrigeration co. LTD. Her main research fields are fundamentals of characteristics of two-phase flow in helically coiled channel, measurement technology of electric conductivity, sealing technology in single screw expander, air conditioning and ventilation technology, and fluid-structure interaction.



Guodong Xia is a leading professor in Thermal Energy Engineering at Beijing University of Technology, China. He received his Ph.D. in Thermal Energy Engineering at the State Key Laboratory of Multiphase Flow of Xi'an Jiaotong University, China in 1996. He was a visiting professor in the Institute of Process Engineering at the University of Hanover, Germany in 2000 -2001. His research interests include fundamentals and applications of microscale heat transfer, multiphase flow and heat transfer, waste energy recovery, thermal energy system, heat exchanger design and enhanced heat transfer. He is a member of the multiphase flow committee of the Chinese Society of Engineering Thermophysics and a member of the multiphase flow committee of the Chinese Society of Theoretical and Applied Mechanics. He has published more than 150 papers in journals and conferences.



Lixin Cheng has worked at Sheffield Hallam University since 2016. He obtained his Ph.D. in Thermal Energy Engineering at the State Key Laboratory of Multiphase Flow at Xi'an Jiaotong University, China in 1998. He has received several prestigious awards such as Alexander von Humboldt Fellowship in Germany in 2006, an ERCOFTAC Visitor Grant in Switzerland in 2010 and a Distinguished Visiting Professorship of the City of Beijing, China in 2015. His research interests include multiphase flow and heat transfer and thermal energy engineering. He has published more than 100 papers in journals and conferences, 9 book chapters and edited 10 books. He has delivered more than 60 keynote and invited lectures worldwide. He has been the chair of the *World Congress on Momentum, Heat and Mass Transfer (MHMT)* since 2017. He is one of the founders and co-chair of the *International Symposium of Thermal-Fluid Dynamics (ISTFD)* series since 2019. He is associate editor of *Heat Transfer Engineering* and *Journal of Fluid Flow, Heat and Mass Transfer*, and international advisor of *Thermal Power Generation* (a Chinese journal).



Zhipeng Wang is an intermediate engineer in the Tianjin Lantian Solar Technology Co. Ltd. He received his Master Degree in Beijing University of Technology in China. He is devoted to the investigation of the multiphase flow and heat transfer, and thermal design of the electronic devices.